

Exact treatment of trapped imbalanced fermions in the BEC limit

P. PIERI AND G.C. STRINATI

Dipartimento di Fisica, Università di Camerino, I-62032 Camerino, Italy

1. – Introduction

In the present contribution we shall analyze the effects of imbalancing the populations of two-component trapped fermions in the BEC (strong-coupling) limit of the attractive interaction between fermions of different components. In particular, we shall derive a set of coupled equations which describe composite bosons and excess fermions in this limit, starting from the gap equation with two different fermionic chemical potentials. Care will be used to include in these equations the processes leading to the correct dimer-dimer and dimer-fermion scattering lengths, which require us to consider beyond-mean-field effects. Numerical results will be presented for the density profiles of composite bosons and excess fermions, which are relevant to the recent experiments with trapped Fermi atoms. Results for the formation of vortex patterns in the presence of density imbalance will also be presented.

The interest in imbalanced populations of fermions with different spins originated long time ago from condensed-matter physics, where a magnetic field can alter the populations of spin \uparrow and \downarrow electrons [1, 2].

Quite generally, density imbalance $\delta n = n_{\uparrow} - n_{\downarrow}$ between “spin up” and “spin down” fermions introduces *a new degree of freedom* in the system, and may thus possibly lead to the removal degeneracies and the occurrence of novel phases [3, 4].

In this context, trapped cold Fermi atoms offer a unique possibility for observing the consequences of density imbalance. These systems has lately be object of mounting interest, both experimentally and theoretically, as they allow one to explore the BCS-BEC

crossover by controlling the interaction between fermions of different components via the use of Fano-Feshbach resonances. Recently, two experimental studies with imbalanced populations have raised novel interest in these systems [5, 6]. Density profiles of the two fermionic species as well as vortices have been detected. A quantum phase transition to the normal state on the BCS side of the crossover as well as phase separation in the crossover region have been identified.

From a theoretical point of view, the BCS-BEC crossover gets modified as the many-body problem becomes richer in the presence of density imbalance. The interest in this problem has then involved not only cold-atom and condensed-matter physics, but also nuclear and subnuclear physics. On the BEC side of the crossover, it further gives one the opportunity of embedding into the diagrammatic structure the processes [7, 8] leading to the correct values of the scattering lengths for two composite bosons (a_B) and for a composite boson with an excess fermion (a_{BF}).

The effects of density imbalance on fermionic superfluids were originally studied in the weak-coupling (BCS) limit of the crossover both for the homogeneous [9] and trapped case [10]. Only recently these calculations have been extended to cover the BCS-BEC crossover [11], and to consider the effects of the trap [12, 13, 14] which are essential to account for the experimental results with density imbalance. We thus begin by giving in the next Section a brief account of the mean-field approach for the homogenous case when different spin populations are considered, with emphasis to the strong-coupling (BEC) limit to which we shall eventually restrict in the later Sections when considering the trapped case.

2. – Mean-field treatment for the homogeneous case

The microscopic BCS theory of superconductivity is most conveniently formulated in terms of fermionic single-particle Green's functions [15]. Due to the presence of spontaneous broken symmetry, anomalous averages need be considered together with normal averages, leading to a 2×2 matrix for the Green's functions.

This formulation can be readily extended to include different populations for the two fermionic species (labeled by spin- \uparrow and spin- \downarrow) which mutually interact via a contact potential. This is done by considering two different chemical potentials μ_\uparrow and μ_\downarrow for the two species, so that the *equation of motion* for the fermionic single-particle Green's functions $G_{ij}(\mathbf{k}, \omega_s)$ within mean field reads:

$$(1) \quad \begin{bmatrix} i\omega_s - \frac{\mathbf{k}^2}{2m} + \mu_\uparrow & -\Delta \\ -\Delta^* & i\omega_s + \frac{\mathbf{k}^2}{2m} - \mu_\downarrow \end{bmatrix} \begin{bmatrix} G_{11} & G_{12} \\ G_{21} & G_{22} \end{bmatrix} = \begin{bmatrix} 1 & 0 \\ 0 & 1 \end{bmatrix}.$$

Here, $\omega_s = (2s+1)\pi/(k_B T)$ (s integer) is a fermionic Matsubara frequency at temperature T , \mathbf{k} a wave vector, m the fermion mass, and Δ the gap function. The novelty introduced in eq. (1) by population imbalance is the presence of two different chemical potentials in

the diagonal matrix elements on its left-hand side. This seemingly minor difference will, however, yield significant different results upon inverting eq. (1) in favor of G_{ij} .

From this inversion one obtains, in particular:

$$(2) \quad \begin{aligned} n &= n_{\uparrow} + n_{\downarrow} = \sum_k [e^{i\omega_s\eta} G_{11}(k) - e^{-i\omega_s\eta} G_{22}(k)] \\ &= \int \frac{d\mathbf{k}}{(2\pi)^3} \left\{ 1 - \frac{\xi(\mathbf{k})}{E(\mathbf{k})} [1 - f(E_+(\mathbf{k})) - f(E_-(\mathbf{k}))] \right\} \end{aligned}$$

for the total density (where η is a positive infinitesimal),

$$(3) \quad \begin{aligned} \delta n &= n_{\uparrow} - n_{\downarrow} = \sum_k [e^{i\omega_s\eta} G_{11}(k) + e^{-i\omega_s\eta} G_{22}(k)] \\ &= \int \frac{d\mathbf{k}}{(2\pi)^3} \{f(E_+(\mathbf{k})) - f(E_-(\mathbf{k}))\} \end{aligned}$$

for the density difference, and

$$(4) \quad -\frac{m}{4\pi a_F} = \int \frac{d\mathbf{k}}{(2\pi)^3} \left\{ \frac{1 - f(E_+(\mathbf{k})) - f(E_-(\mathbf{k}))}{2E(\mathbf{k})} - \frac{m}{\mathbf{k}^2} \right\}$$

for the gap equation where the strength of the contact fermionic attraction has been replaced by the fermionic scattering length a_F by suitable regularization [16]. In these expressions, $f(E) = (e^{\beta E} + 1)^{-1}$ is the Fermi distribution function with $\beta = 1/(k_B T)$ and we have introduced the notation:

$$(5) \quad E_{\pm}(\mathbf{k}) = E(\mathbf{k}) \pm \delta\xi \quad , \quad E(\mathbf{k}) = \sqrt{\xi(\mathbf{k})^2 + |\Delta|^2}$$

and

$$(6) \quad \xi(\mathbf{k}) = \frac{\mathbf{k}^2}{2m} - \frac{\mu_{\uparrow} + \mu_{\downarrow}}{2} \quad , \quad \delta\xi = \frac{\mu_{\downarrow} - \mu_{\uparrow}}{2}$$

[only the case of equal fermion masses will be considered throughout]. Note from eq. (3) that, in the low temperature limit, the only way to sustain a nonvanishing value of δn is to have either $E_+(\mathbf{k})$ or $E_-(\mathbf{k})$ negative. For definiteness, we shall assume $n_{\uparrow} \geq n_{\downarrow}$.

It is known from the theory of the BCS-BEC crossover that the dimensionless parameter $(k_F a_F)^{-1}$ controls the evolution from the weak-coupling BCS regime (where $a_F < 0$ and $(k_F a_F)^{-1} \lesssim -1$) to the strong-coupling BEC regime (where $a_F > 0$ and $(k_F a_F)^{-1} \gtrsim +1$), with the “crossover” region being limited in practice to the interval $-1 \lesssim (k_F a_F)^{-1} \lesssim +1$. Here, k_F is the Fermi wave vector related in the standard way to the total density.

In the following, we shall mostly be interested in the strong-coupling (BEC) regime at low temperature. In this limit, one expects the presence of density imbalance to produce a density n_{\downarrow} of composite bosons formed by pairing a fermion of spin \uparrow with a fermion

of spin \downarrow , plus a density $\delta n = n_{\uparrow} - n_{\downarrow}$ of excess fermions of spin \uparrow . Correspondingly, one finds from eqs. (2)-(3):

$$(7) \quad \mu_{\downarrow} = -\epsilon_0 - \mu_{\uparrow} + \mu_B$$

where $\epsilon_0 = \frac{1}{m a_F^2}$ is the binding energy of the associated two-body problem and

$$(8) \quad \mu_{\uparrow} \cong \epsilon_F(\delta n) + \left(\frac{2\pi a_{BF}}{m_{BF}} \right) n_0$$

$$(9) \quad \mu_B \cong \left(\frac{4\pi a_B}{m_B} \right) n_0 + \left(\frac{2\pi a_{BF}}{m_{BF}} \right) \delta n .$$

In these expressions, $\epsilon_F(\delta n)$ is the Fermi energy corresponding to δn , μ_B plays the role of the chemical potential of the composite bosons, and n_0 is the condensate density which equals $(n - \delta n)/2$ under the present circumstances. In addition, $m_B = 2m$ is the mass of a composite boson, $m_{BF} = \frac{2}{3}m$ is the reduced mass of the two-body system made up of a composite boson and an excess fermion, while $a_B = 2a_F$ is the scattering length for the scattering of two composite bosons and $a_{BF} = (8/3)a_F$ for the scattering of a composite boson and an excess fermion. These values for a_B and a_{BF} are specific to the mean-field treatment and correspond to the Born approximation for the scattering processes.

After these preliminary considerations of general relevance in the presence of imbalanced fermion populations, we pass now to consider the trapped case which is specifically relevant to the experiments with cold atoms.

3. – Mean-field treatment for the trapped case

At a formal level the mean-field treatment for the inhomogeneous case proceeds along similar lines as for the homogenous case discussed in the previous Section, the difference being that the *equation of motion* for the fermionic single-particle Green's functions $G_{ij}(\mathbf{r}, \mathbf{r}'; \omega_s)$ is now given by:

$$(10) \quad \begin{bmatrix} i\omega_s - \mathcal{H}_{\uparrow}(\mathbf{r}) & -\Delta(\mathbf{r}) \\ -\Delta(\mathbf{r})^* & i\omega_s + \mathcal{H}_{\downarrow}(\mathbf{r}) \end{bmatrix} \begin{bmatrix} G_{11} & G_{12} \\ G_{21} & G_{22} \end{bmatrix} = \delta(\mathbf{r} - \mathbf{r}') \begin{bmatrix} 1 & 0 \\ 0 & 1 \end{bmatrix} .$$

Here, $\mathcal{H}_{\sigma}(\mathbf{r}) = -\frac{\nabla^2}{2m} + V(\mathbf{r}) - \mu_{\sigma}$ is the single-particle Hamiltonian in the presence of the trapping potential $V(\mathbf{r})$. Equation (10) is the Green's function version of the Bogoliubov-de Gennes equations [17], which are often used to describe inhomogeneous superconductors.

As in the previous Section, we are mostly interested in the strong-coupling BEC regime at low temperature. In the case of equal fermion populations (whereby $\mu_{\uparrow} = \mu_{\downarrow}$), it has been shown [18] that the Gross-Pitaevskii equation for composite bosons can be derived in this limit from the Bogoliubov-de Gennes equations (10). This mapping enables one to

exploit the results obtained directly from the more manageable bosonic Gross-Pitaevskii equation and, when needed, to use them as benchmarks for the fermionic calculation in the limit. This analysis has recently been extended to the imbalanced case when $\mu_\uparrow \neq \mu_\downarrow$. In this case, in the place of the Gross-Pitaevskii equation one ends up with two coupled equations that describe the simultaneous presence of composite bosons and excess fermions [12]. As the analysis proceeds along similar lines in both (balanced and imbalanced) cases, we indicate it here schematically for convenience.

One starts by rewriting the Bogoliubov-de Gennes equations (10) in the integral form:

$$(11) \quad \hat{\mathcal{G}}(\mathbf{r}, \mathbf{r}'; \omega_s) = \hat{\mathcal{G}}_0(\mathbf{r}, \mathbf{r}'; \omega_s) + \int d\mathbf{r}'' \hat{\mathcal{G}}_0(\mathbf{r}, \mathbf{r}''; \omega_s) \hat{B}(\mathbf{r}'') \hat{\mathcal{G}}(\mathbf{r}'', \mathbf{r}'; \omega_s)$$

where

$$(12) \quad \hat{\mathcal{G}}_0(\mathbf{r}, \mathbf{r}'; \omega_s) = \begin{bmatrix} \tilde{\mathcal{G}}_0(\mathbf{r}, \mathbf{r}'; \omega_s | \mu_\uparrow) & 0 \\ 0 & -\tilde{\mathcal{G}}_0(\mathbf{r}', \mathbf{r}; -\omega_s | \mu_\downarrow) \end{bmatrix}$$

is the matrix of the noninteracting Green's functions which satisfy the equation

$$(13) \quad [i\omega_s - \mathcal{H}_\sigma(\mathbf{r})] \tilde{\mathcal{G}}_0(\mathbf{r}, \mathbf{r}'; \omega_s | \mu_\sigma) = \delta(\mathbf{r} - \mathbf{r}'),$$

being subject to the same trapping potential $V(\mathbf{r})$ entering the single-particle Hamiltonian $\mathcal{H}_\sigma(\mathbf{r})$. In addition, the matrix

$$(14) \quad \hat{B}(\mathbf{r}) = \begin{bmatrix} 0 & \Delta(\mathbf{r}) \\ \Delta^*(\mathbf{r}) & 0 \end{bmatrix}$$

contains the effects of the interaction via the gap function.

At this point, expansion of $\mathcal{G}_{11}(\mathbf{r}, \mathbf{r}'; \omega_s)$ and $\mathcal{G}_{22}(\mathbf{r}, \mathbf{r}'; \omega_s)$ up to order Δ^2 yields the expressions for the local densities $n_\uparrow(\mathbf{r})$ and $n_\downarrow(\mathbf{r})$, in the order, while expansion of $\mathcal{G}_{12}(\mathbf{r}, \mathbf{r}'; \omega_s)$ up to order Δ^3 yields an equation for the local gap $\Delta(\mathbf{r})$. The gap equation can be cast in the form [12]:

$$(15) \quad -\frac{\nabla^2}{2m_B} \Phi(\mathbf{r}) + \left[2V(\mathbf{r}) + \frac{3\pi a_{\text{BF}}}{m} \delta n(\mathbf{r}) \right] \Phi(\mathbf{r}) + \frac{4\pi a_B}{m_B} |\Phi(\mathbf{r})|^2 \Phi(\mathbf{r}) = \mu_B \Phi(\mathbf{r})$$

where again $m_B = 2m$, $a_B = 2a_F$, $a_{\text{BF}} = \frac{8}{3}a_F$, $\mu_B = \mu_\uparrow + \mu_\downarrow + \epsilon_0$, while $\Phi(\mathbf{r}) = \sqrt{\frac{m^2 a_F}{8\pi}} \Delta(\mathbf{r})$ plays the role of the bosonic *condensate wave function*.

By a similar token, the density of excess fermions reads:

$$(16) \quad \delta n(\mathbf{r}) = n_\uparrow(\mathbf{r}) - n_\downarrow(\mathbf{r}) \cong \int \frac{d\mathbf{k}}{(2\pi)^3} f \left(\frac{\mathbf{k}^2}{2m} + V(\mathbf{r}) + \frac{3\pi a_{\text{BF}}}{m} |\Phi(\mathbf{r})|^2 - \mu_\uparrow \right).$$

Note that the two coupled equations (15) and (16) embody the mutual effects of the bosonic distribution $|\Phi(\mathbf{r})|^2$ and the fermionic distribution $\delta n(\mathbf{r})$. Finally, the expression

for the density is:

$$(17) \quad n(\mathbf{r}) = n_{\uparrow}(\mathbf{r}) + n_{\downarrow}(\mathbf{r}) = \delta n(\mathbf{r}) + 2|\Phi(\mathbf{r})|^2$$

which completes the set of three coupled equations for $\Phi(\mathbf{r})$, $\delta n(\mathbf{r})$, and $n(\mathbf{r})$.

The remaining problem is that the scattering between composite bosons (as embodied by a_B) and between a composite boson and an excess fermion (as embodied by a_{BF}) has been treated so far at the lowest order within the Born approximation, corresponding to the values $a_B = 2a_F$ and $a_{BF} = \frac{8}{3}a_F$ obtained by our derivation. This points to the need of going beyond the mean-field treatment to include the full set of scattering processes for a_B and a_{BF} . In diagrammatic language, this implies identifying additional fermionic diagrams containing diagrammatic sequences for a_B and a_{BF} as sub-units.

4. – Exact equations in the dilute case

The validity of the equations obtained in the previous Section can be extended by improving on the values of the scattering lengths a_B and a_{BF} . From the exact solutions (in real-space representation) of the three- [19] and four-body [20] problems it is known that the correct values are $a_{BF} = 1.18a_F$ and $a_B = 0.6a_F$, in the order. These values have also been determined *diagrammatically* (in wave-vector representation) in the limit of vanishing density, for a_{BF} in ref. [8] and for a_B in ref. [7]. To improve on the derivation of the equations obtained in the previous Section, one has thus to embed the diagrammatic sub-units, which identify a_B and a_{BF} in the limit of vanishing density, into the many-body structure at finite density. This can be achieved as follows.

As a natural extension of what is done for determining the condensate density of point-like bosons [21], in the BEC limit of interest here the gap equation can be interpreted as the condition of vanishing “tadpole” insertions for composite bosons. At the mean-field level considered in the previous Section, the diagrams representing this condition are depicted in fig. 1(a), with the understanding that a composite-boson propagator with zero four-momentum can be inserted from the left while the gap Δ corresponds to a condensate line. These diagrams account for the dimer-fermion and dimer-dimer scattering processes within the Born approximation. The additional tadpole diagrams, which yield the correct values of a_{BF} and a_B , are depicted in figs. 1(b) and 1(c), in the order. Here, the dimer-fermion and dimer-dimer scattering processes exclude the Born-approximation contributions already included at the mean-field level in fig. 1(a).

With this procedure, one ends up formally with the same coupled equations (15)-(17) which, however, now contain the correct values of a_B and a_{BF} . In this context, a comment is worth on how to factor out from the diagrams of fig. 1(b) the product a_{BF} times δn that enters eq. (15). The point is that the integration over the wave vector \mathbf{P} is bounded within the Fermi sphere of radius $\sqrt{2m\mu_{\uparrow}}$, while the remaining integrations over \mathbf{q} , \mathbf{q}' , \dots , extend outside this Fermi sphere. One may, accordingly, neglect the P -dependence everywhere in the diagrams of fig. 1(b) *except* in the fermion propagator labeled by P and corresponding to spin- \uparrow fermions. The density of excess fermions results

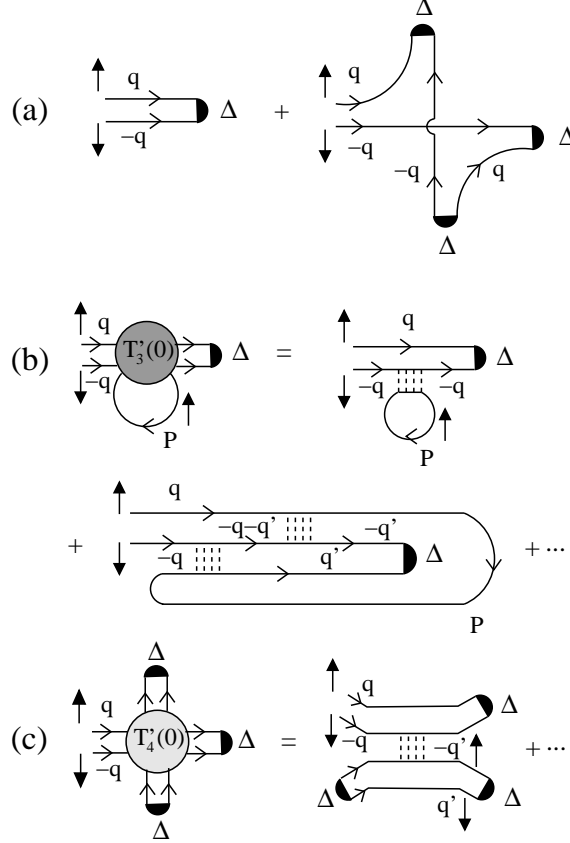


Fig. 1. – Tadpole diagrams for composite bosons describing the gap equation in the BEC limit. (a) Mean-field contributions; Contributions beyond the Born approximation which include the scattering processes yielding the correct values of the (b) dimer-fermion and (c) dimer-dimer scattering lengths. Full lines represent the fermion propagators of given spin and broken lines represent the bare fermionic interaction. [Reproduced from ref. [12].]

in this way from the P -integration, with the remaining parts of the diagrams yielding the exact dimer-fermion scattering matrix $T'_3(0)$. This excludes, by definition, the Born contribution resulting from mean field. A similar analysis can be carried out for the density equation (16), where only the value of the dimer-fermion scattering length a_{BF} requires corrections beyond mean field [12].

5. – Numerical results and comparison with experiments

We pass now to report on the numerical solution of the coupled equations (15)-(17) with the exact values of a_B and a_{BF} . By their very derivation, these equations are expected to be valid in the strong-coupling (BEC) regime where $a_F > 0$, which however

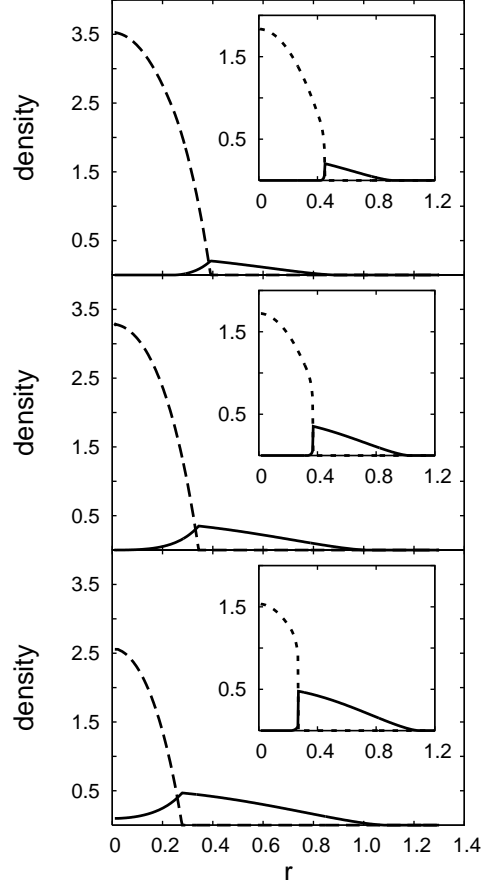


Fig. 2. – Density profiles $\delta n(r)$ (full lines) and $n_0(r)$ (broken lines) vs. r for $(k_F a_F)^{-1} = 3$ and $\alpha = 0.2$ (upper panel), $\alpha = 0.5$ (middle panel), $\alpha = 0.8$ (lower panel). The insets show the results when $(k_F a_F)^{-1} = 1$ for the same values of α . Here, r is in units of R_{TF} and densities are in units of $(N_{\uparrow} + N_{\downarrow})/R_{\text{TF}}^3$. The Thomas-Fermi radius R_{TF} and the Fermi wave vector k_F are defined for equal populations. [Reproduced from ref. [12].]

extends as down as to $(k_F a_F)^{-1} \approx +1$ for all practical purposes.

We determine the density profiles $\delta n(\mathbf{r})$ and $n_0(\mathbf{r}) = |\Phi(\mathbf{r})|^2$ in the Thomas-Fermi (LDA) approximation (which corresponds to neglecting the kinetic energy term in eq. (15)) for a spherical trap, as functions of the *asymmetry parameter* $\alpha = (N_{\uparrow} - N_{\downarrow})/(N_{\uparrow} + N_{\downarrow})$ (where $0 \leq \alpha \leq 1$). Numerical results [12] are shown in:

(i) fig. 2 for the density profiles $\delta n(r)$ and $n_0(r)$ vs. the distance $r = |\mathbf{r}|$ from the center of the trap, for three characteristic values of α and for the coupling $(k_F a_F)^{-1} = 3$ on the BEC side of the crossover. The insets show the results for the smaller coupling $(k_F a_F)^{-1} = 1$. A spatial separation results between the condensed composite bosons

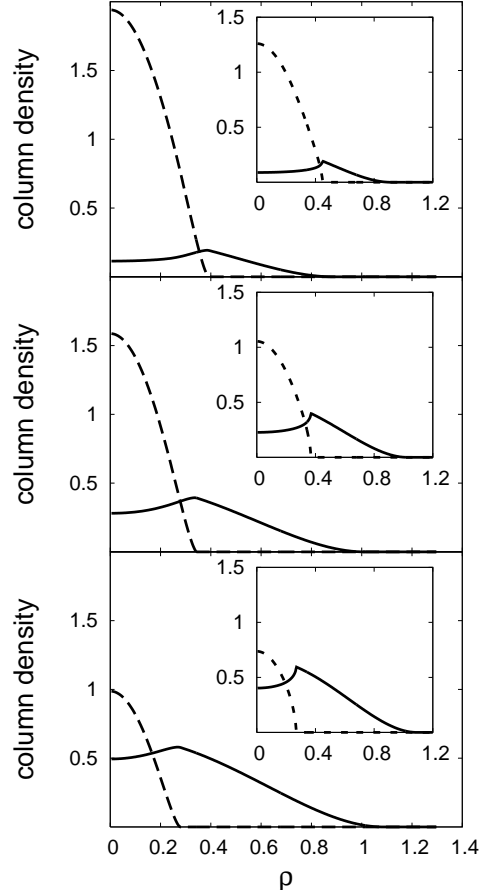


Fig. 3. – Column density profiles $\delta n(\rho)$ (full lines) and $n_0(\rho)$ (broken lines) vs. ρ for $(k_F a_F)^{-1} = 3$ and $\alpha = 0.2$ (upper panel), $\alpha = 0.5$ (middle panel), $\alpha = 0.8$ (lower panel). The insets show the results when $(k_F a_F)^{-1} = 1$ for the same values of α . Here, ρ is in units of R_{TF} and densities are in units of $(N_\uparrow + N_\downarrow)/R_{\text{TF}}^2$.

and the excess fermions, which appears sharper for the smaller coupling, corresponding to enhanced effects of the dimer-fermion repulsion. Upon approaching unitarity $[(k_F a_F)^{-1} = 0]$, there thus appears a tendency toward *phase separation* with a superconducting core of fully paired fermions surrounded by a cloud of excess fermions. For the couplings here considered, this phase separation occurs for all values of α . Note that, for each value of α , the maximum of $\delta n(r)$ occurs where $n_0(r)$ vanishes, and that there occurs a progressive size shrinking of $n_0(r)$ for increasing α , with a simultaneous penetration of $\delta n(r)$ toward the center of the trap.

(ii) fig. 3 for the corresponding *column* density profiles $n(\rho) = \int dz n(\rho, z)$ vs. $\rho = \sqrt{x^2 + y^2}$. Phase separation appears now less visible even for $(k_F a_F)^{-1} = 1$, since $n(\rho)$

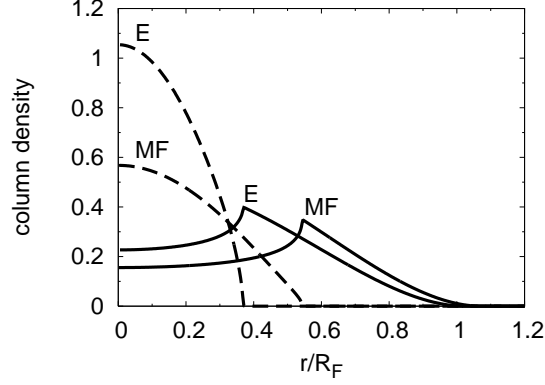


Fig. 4. – Column density profiles $\delta n(\rho)$ (full lines) and $n_0(\rho)$ (broken lines) vs. ρ when $(k_F a_F)^{-1} = 1$ and $\alpha = 0.5$, as obtained with the exact (E) and mean-field (MF) values of the scattering lengths. Units are the same as in fig. 3.

leaks toward $\rho = 0$ where it acquires a finite value.

(iii) fig. 4 for the comparison of the column density profiles when $(k_F a_F)^{-1} = 1$ and $\alpha = 0.4$, as obtained with the exact and mean-field values of the scattering lengths. The use of the exact values of the scattering lengths results in density profiles which are more compressed toward $\rho = 0$. This feature can be conveniently characterized by the values of the *critical radius* R_c where the condensate vanishes.

(iv) fig. 5 for the critical radius R_c of the condensate density, which is plotted vs. α for different couplings and using the exact (a) or mean-field (b) values of the scattering lengths. This quantity identifies also the position of the maximum of the density of excess

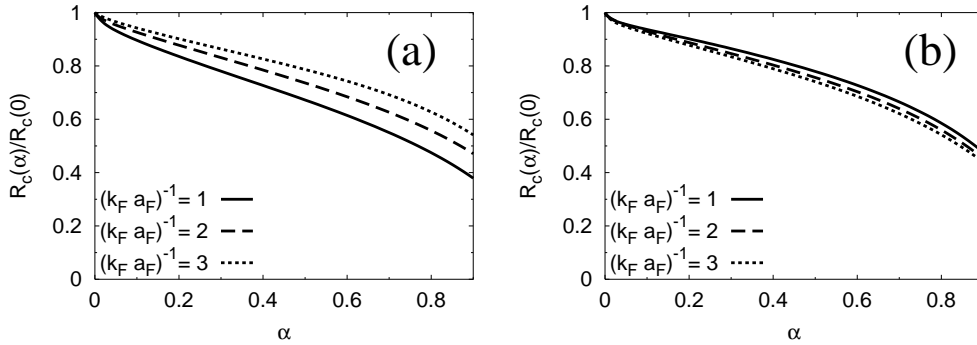


Fig. 5. – Critical radius R_c of the condensate density vs. the asymmetry parameter α (normalized to the value $R_c(0)$ at $\alpha = 0$) for three coupling values, obtained by using the exact (a) or mean-field (b) values of the scattering lengths. [Adapted from ref. [12].]

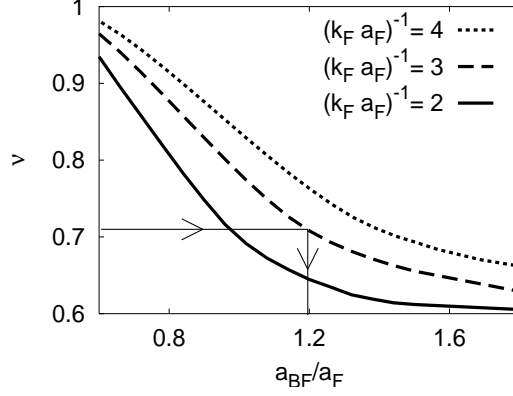


Fig. 6. – Ratio ν between the column density of excess fermions at the center of the trap and its maximum value at R_c vs. the ratio a_{BF}/a_F , for $\alpha = 0.5$ and three coupling values. [Adapted from ref. [12].]

fermions. Note the inverted sequence of the curves corresponding to the different values of $(k_F a_F)^{-1}$, as calculated with the exact or with the mean-field values of the scattering lengths. This feature could be subject to experimental verification.

(v) fig. 6 for the ratio ν between the column density of the excess fermions at the center of the trap and its maximum value at the critical radius R_c vs. a_{BF}/a_F for $\alpha = 0.5$ and different couplings. The use of column density to obtain the ratio ν stems from our finding that column density profiles have a more marked dependence on a_{BF} . Indeed, the marked dependence on a_{BF} should make it possible to extract the expected value 1.18 of a_{BF}/a_F from the experimental data, using the plots of fig. 6 as *calibration curves*. This procedure is indicated schematically in the figure.

Note that, although the results presented in this Section have been obtained for an isotropic (spherical) trap, they can be also utilized for an anisotropic (ellipsoidal) trap, as indicated in Appendix A.

Comparison with the experimental results by the MIT [5] and Rice [6] groups for the density profiles of the two imbalanced fermion species can be established at this point, at least as far as the BEC side of the crossover region is concerned. In this regime and at low temperatures, the experiments indicate that the dominant effect of density imbalance is to phase separate the system in two components, with an inner superfluid region where fermions of different species balance each other and an outer normal region where the excess fermions reside. This effect was correctly reported for the first time in ref. [12] and it is clearly evidenced in the above figures.

6. – Extension to vortices (rotating frame)

Unambiguous detection of the superfluid phase for trapped Fermi atoms with balanced populations has been achieved by the observation of vortex lattices when the system is put into *rotation* [22]. By a similar token, in the presence of density imbalance between the two fermionic species, detection of the superfluid region has relied on the observation of vortices in that region [5].

To deal with vortex patterns originating from fermions in the presence of density imbalance, we extend the previous treatment holding on the BEC side of the crossover in the following way. We begin by noting that the two coupled equations (15) and (16) for the condensate wave function $\Phi(\mathbf{r})$ and the density of excess fermions $\delta n(\mathbf{r})$ could alternatively be derived from a suitable *energy functional* $E[\Phi, \delta n]$. When the system is further put into rotation, this energy functional reads:

$$\begin{aligned}
 E[\Phi, \delta n] = Z \int dxdy \left\{ \frac{1}{4m} |\nabla \Phi(\mathbf{r})|^2 + m\omega_r^2 r^2 |\Phi(\mathbf{r})|^2 + \frac{\pi a_B}{m} |\Phi(\mathbf{r})|^4 \right. \\
 - \Omega \Phi(\mathbf{r})^* L_z \Phi(\mathbf{r}) + \frac{6^{5/3} \pi^{4/3}}{20m} \delta n(\mathbf{r})^{5/3} + \frac{1}{2} m\omega_r^2 r^2 \delta n(\mathbf{r}) \\
 \left. + \frac{3\pi a_{BF}}{m} |\Phi(\mathbf{r})|^2 \delta n(\mathbf{r}) - \frac{1}{2} m\Omega^2 r^2 \delta n(\mathbf{r}) \right\}.
 \end{aligned}
 \tag{18}$$

Here, Ω is the rotation frequency, L_z the angular momentum operator of the composite bosons, $\mathbf{r} = (x, y, 0)$, while for calculation convenience the original ellipsoidal trap has been replaced by a cylinder of height Z with a harmonic radial potential. Note that in eq. (18) the excess fermions in the rotating frame have been treated within a semi-classical description. Let, in fact,

$$n_R(\mathbf{r}) = \int \frac{d\mathbf{p}}{(2\pi\hbar)^3} \frac{1}{e^{\beta[\epsilon_R(\mathbf{p}, \mathbf{r}) - \mu]} + 1}
 \tag{19}$$

be the semi-classical fermionic distribution in the rotating (R) frame, where $\epsilon_R(\mathbf{p}, \mathbf{r}) = \frac{\mathbf{p}^2}{2m} + U(\mathbf{r}) - \boldsymbol{\Omega} \cdot \mathbf{l}$ the associated semi-classical dispersion with angular momentum \mathbf{l} . Since the last expression can be manipulated as follows

$$\begin{aligned}
 \epsilon_R(\mathbf{p}, \mathbf{r}) &= \frac{\mathbf{p}^2}{2m} + U(\mathbf{r}) - \mathbf{p} \cdot (\boldsymbol{\Omega} \times \mathbf{r}) \\
 &= \frac{\mathbf{p}'^2}{2m} + U(\mathbf{r}) - \frac{1}{2} m(\boldsymbol{\Omega} \times \mathbf{r})^2
 \end{aligned}
 \tag{20}$$

where $\mathbf{p}' = \mathbf{p} - m\boldsymbol{\Omega} \times \mathbf{r}$ in the last line, eq. (19) can eventually be cast in the form:

$$n_R(\mathbf{r}) = \int \frac{d\mathbf{p}'}{(2\pi\hbar)^3} f \left(\frac{\mathbf{p}'^2}{2m} + U(\mathbf{r}) - \frac{1}{2} m(\boldsymbol{\Omega} \times \mathbf{r})^2 \right)
 \tag{21}$$

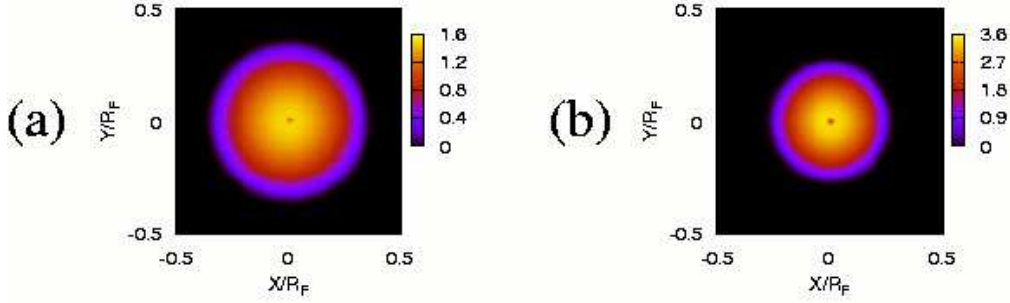


Fig. 7. – Pattern of an isolated vortex in the balanced situation ($\alpha = 0$) at the lower critical frequency for coupling values (a) $(k_F a_F)^{-1} = 1$ and (b) $(k_F a_F)^{-1} = 4$.

which agrees with the expression for $\delta n(\mathbf{r})$ one obtains from eq. (18).

Sticking to this equation, one has the choice of *either* solving the associated coupled differential equations for $\Phi(\mathbf{r})$ and $\delta n(\mathbf{r})$ *or* minimizing directly $E[\Phi, \delta n]$ by varying $\Phi(\mathbf{r})$ and $\delta n(\mathbf{r})$. In practice, a “mixed” approach may sometimes be preferred [23]. Note that in the present treatment the Thomas-Fermi (LDA) approximation is altogether avoided. [We have also verified that this refinement leads only to minor changes for the density profiles presented in Section 5 in the absence of rotation.]

We present numerical results for the parameters of the MIT trap [5] for which $N = 2 \times 10^6$, $\omega_\perp = 57Hz$, and $\omega_z = 23Hz$. We begin by showing in fig. 7 the pattern of an isolated vortex in the balanced ($\alpha = 0$) situation at the lower critical frequency Ω_{c1} when the first vortex enters the system, for the two cases $(k_F a_F)^{-1} = 1$ and $\Omega_{c1} = 3.95Hz$

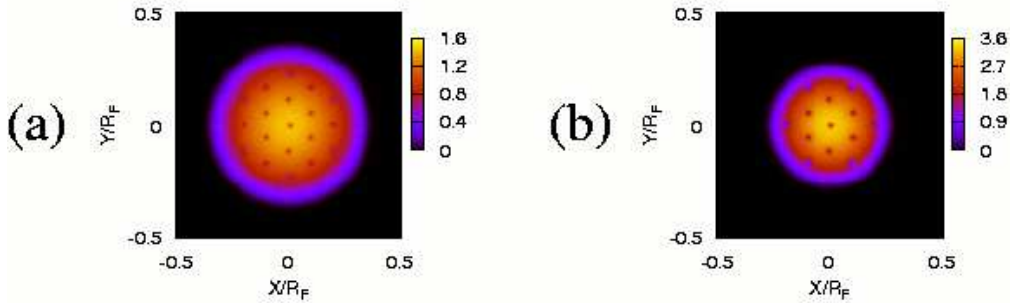


Fig. 8. – Triangular-shape vortex lattice in the balanced situation ($\alpha = 0$) when $\Omega = 19Hz$ and for coupling values (a) $(k_F a_F)^{-1} = 1$ and (b) $(k_F a_F)^{-1} = 4$.

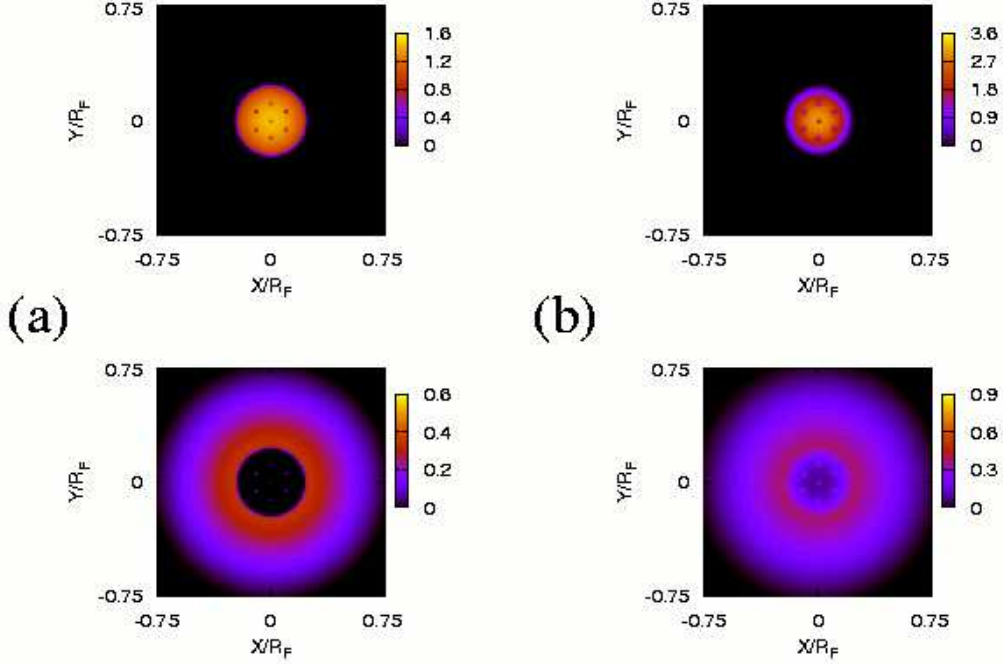


Fig. 9. – Triangular-shape vortex lattice in the imbalanced situation with $\alpha = 0.4$, $\Omega = 19Hz$, and coupling values (a) $(k_F a_F)^{-1} = 1$ and (b) $(k_F a_F)^{-1} = 4$. The upper (lower) plots refer to the density of condensed composite bosons (excess fermions).

(a), and $(k_F a_F)^{-1} = 4$ and $\Omega_{c_1} = 6.11Hz$ (b). When the rotation frequency increases further, this pattern evolves in a triangular-shape vortex lattice shown in fig. 8 when $\Omega = 19Hz$ for the same coupling values as in fig. 7. Such triangular pattern persists in the imbalanced situation, as shown in fig. 9 for $\alpha = 0.4$ and the same frequency $\Omega = 19Hz$, when (a) $(k_F a_F)^{-1} = 1$ and (b) $(k_F a_F)^{-1} = 4$. In fig. 9 the *upper* plots picture the density of condensed composite bosons while the *lower* plots refer to excess fermions. Note that the excess fermions tend to pile up in the vortex cores, taking thus advantage of the fact that the density of composite bosons is depressed there. Further study along these lines is in progress [23].

7. – Perspectives and open problems

In this contribution, we have presented a theoretical account of the effects produced by imbalancing the populations of trapped fermions. Special emphasis has been placed to the strong-coupling (BEC) limit, where theoretical studies can be extended beyond

BCS mean field by exploiting the diluteness condition of the system. Several effects were, however, left out from our analysis.

First of all, it appears relevant to combine density imbalance with *mass imbalance* of the two fermionic species, which may act to promote still novel phenomena in the system and it is being subject to experimental investigations at present.

The present approach was confined to the BEC region where $(k_F a_F)^{-1} \gtrsim +1$. As the experiments [5, 6] actually span the whole crossover region $-1 \lesssim (k_F a_F)^{-1} \lesssim +1$, theoretical calculations should cover this region, too. In this context, a mean-field approach could readily produce a qualitative overview of the effects taking place across the crossover region, including both density and mass imbalance. As in the case of the BEC region, however, mean-field calculations may lead to quantitative incorrect results. For instance, at unitarity and for $T \simeq 0$, mean-field calculations [14] result in the value $\alpha_c^{MF} \simeq 1$ for the critical asymmetry parameter α_c past which the superfluid region disappears from the system, while the experiment [5] yields $\alpha_c^{exp} \simeq 0.70$. This is a clear indication that inclusion of *pairing fluctuations* beyond mean field is relevant in the crossover region to account for the experimental data.

At higher temperatures, density imbalance may give access to “precursor” pairing (pseudo-gap) effects for the excess fermions, which could thus be evidenced in the normal phase *even below* the critical temperature T_c . This may result in a strong suppression of thermal fluctuations, leading to a possible detection of an underlying Quantum Critical Point.

Finally, we mention that a compelling test for theories would result from calculating the dependence of T_c on α , as the experiments were able to determine the temperature of the system directly from the “tail” of the density profiles of the excess fermions [24].

APPENDIX A.

Appendix A: Mapping of the anisotropic onto the isotropic problem

The calculations presented in Section 5 refer to an isotropic harmonic potential (spherical trap). In the experiments with cold Fermi atoms, however, anisotropic harmonic traps are most often used. The question thus naturally arises to what an extent the theoretical calculations done for a spherical trap can account for the experimental situation.

The answer to this question relies on the validity of the Thomas-Fermi (LDA) approximation, which applies when the number N of trapped atoms is large enough and was explicitly used in the calculations of Section 5. [As a matter of fact, when N is large enough, avoiding this approximation leads only to minor changes of the density profiles, as mentioned in Section 6.]

This is because, within LDA, physical quantities acquire an \mathbf{r} -dependence *only through* the local chemical potential

$$(A.1) \quad \mu(x, y, z) = \mu - \frac{1}{2} m \omega_x^2 (x^2 + \lambda_y^2 y^2 + \lambda_z^2 z^2) .$$

Here, the anisotropy of the harmonic potential is specified by the parameters λ_y and λ_z . In particular, the density profiles of interest can be expressed as $n(x, y, z) = n[\mu(x, y, z)]$.

To establish the desired mapping with the isotropic case, we introduce an *equivalent isotropic problem* with a total number of atoms $N_{\text{iso}} = \lambda_y \lambda_z N$, the harmonic frequency $\omega_{\text{iso}} = \omega_x$, and the same Fermi energy $E_{\text{F}}^{\text{iso}} = E_{\text{F}} = (3\omega_x \omega_y \omega_z N)^{1/3}$ of the original anisotropic problem. To determine the corresponding chemical potential μ_{iso} for this problem, we argue that the ratio $\mu_{\text{iso}}/E_{\text{F}}$ must be a universal function of the dimensionless quantities $(k_{\text{F}} a_{\text{F}})^{-1}$ and T/E_{F} (where, by definition, $k_{\text{F}} = \sqrt{2mE_{\text{F}}}$). This implies that the ratio $\mu_{\text{iso}}/E_{\text{F}}$ can depend on N only via E_{F} . As a consequence, μ_{iso} of the equivalent isotropic problem must coincide with the chemical potential μ of the original anisotropic problem.

For the density profile $n(x, y, z)$ of the original anisotropic problem, this equivalence eventually implies that it can be expressed in terms of the density profile $n_{\text{iso}}(x, Y, Z)$ of the equivalent isotropic problem as follows:

$$(A.2) \quad n(x, y, z) = n_{\text{iso}} \left[\mu_{\text{iso}} - \frac{1}{2} m \omega_{\text{iso}}^2 (x^2 + Y^2 + Z^2) \right]$$

where $Y = \lambda_y y$ and $Z = \lambda_z z$.

APPENDIX B.

Appendix B: Axial density profiles

The density profiles reported in Section 5 were obtained within the Thomas-Fermi (LDA) approximation. This approximation tends to sharpen the density profiles at their edges, but is otherwise appropriate when the number of trapped atoms is large enough. From those results we have also concluded that the dominant effect of density imbalance is to phase separate the system into two components, an inner superfluid region and an outer normal region with excess fermions only.

In this context, an argument was proposed by De Silva and Mueller [25] to evidence the occurrence of phase separation in the density profiles when the trapping potential is *harmonic*. Their argument relies on the validity of the LDA approximation and applies to the *axial* density $n_{\text{A}}(z)$, obtained from the density through a double integration:

$$(B.1) \quad n_{\text{A}}(z) = \int dx dy n(x, y, z) = \pi \int_0^\infty d\rho^2 n(\rho^2 + z^2) = \pi \int_{z^2}^\infty d\zeta n(\zeta)$$

where $\zeta = \rho^2 + z^2$ and $n(\zeta) \geq 0$.

From the last line of eq. (B.1) one readily concludes that $n_{\text{A}}(z)$ is a *decreasing* function of z . In addition, when $n(x, y, z)$ presents a “hole” in the core region (say, for $r < r_0$), $n_{\text{A}}(z)$ is *constant* in that region. This situation is pictured in fig. 10, where schematic plots of the radial density $n(\zeta)$ with a hole in the core region (upper panel) and of the corresponding axial density $n_{\text{A}}(z)$ with a *flat* behavior in the core (lower panel) are shown. This situation is a fingerprint for the occurrence of phase separation and applies to the density profiles shown in the insets of fig. 2.

* * *

We thank Stefano Simonucci, who performed the numerical calculations on vortices and prepared figs. 7-9. This work was partially supported by the Italian MIUR (contract Cofin-2005 “Ultracold Fermi Gases and Optical Lattices”).

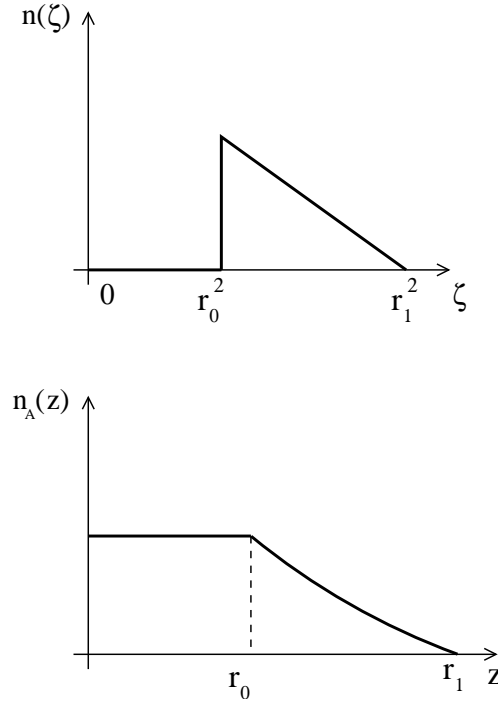


Fig. 10. – Schematic plot of the density $n(\zeta)$ with a hole in the core region and of the corresponding axial density $n_A(z)$ with a flat behavior in the core.

REFERENCES

- [1] CLOGSTON A.M., *Phys. Rev. Lett.*, **9** (1962) 266.
- [2] SARMA G., *J. Phys. Chem. Solids*, **24** (1963) 1029.
- [3] FULDE P. and FERRELL R.A., *Phys. Rev.*, **135** (1964) A550.
- [4] LARKIN A.I. and OVCHINNIKOV Y.N., *Sov. Phys. JETP*, **20** (1965) 762.
- [5] ZWIERLEIN M.W., SCHIROTZEK A., SCHUNCK C.H., and KETTERLE W., *Science*, **311** (2006) 492; SHIN Y., ZWIERLEIN M.W., SCHUNCK C.H., SCHIROTZEK A., and KETTERLE W., *Phys. Rev. Lett.*, **97** (2006) 030401.
- [6] PARTRIDGE G.B., LI W., KAMAR R.I., LIAO Y-AN, and HULET R.G., *Science*, **311** (2006) 503; PARTRIDGE G.B., LI W., LIAO Y.A., HULET R.G., HAQUE M., and STOOF H.T.C., cond-mat/0608455.
- [7] BRODSKY I.V., KLAPTSOV A.V., KAGAN M. YU., COMBESCOT R., and LEYRONAS X., *JETP Letters*, **82** (2005) 273.
- [8] BEDAQUE P.F. and VAN KOLCK U., *Phys. Lett. B*, **428** (1998) 221.
- [9] COMBESCOT R., *Europhys. Lett.*, **55** (2001) 150; LIU W.V. and WILCZEK F., *Phys. Rev. Lett.*, **90** (2003) 047002; CALDAS H., *Phys. Rev. A*, **69** (2004) 063602; SEDRAKIAN A., MUR-PETIT J., POLLS A., and MÜTHER H., *Phys. Rev. A*, **72** (2005) 013613.

- [10] MIZUSHIMA T., MACHIDA K., and ICHIOKA M., *Phys. Rev. Lett.*, **94** (2005) 060404; CASTORINA P., GRASSO M., OERTEL M., URBAN M., and ZAPPALÀ D., *Phys. Rev. A*, **72** (2005) 025601.
- [11] LOMBARDO U., NOZIÈRES P., SCHUCK P., SCHULZE H.-J., and SEDRAKIAN A., *Phys. Rev. C*, **64** (2001) 064314; CARLSON J. and REDDY S., *Phys. Rev. Lett.*, **95** (2005) 060401; PAO C. -H., WU SHIN-TZA, and YIP S.-K., *Phys. Rev. B*, **73** (2006) 132506; SHEEHY D.E. and RADZIHOVSKY L., *Phys. Rev. Lett.*, **96** (2006) 060401.
- [12] PIERI P. and STRINATI G.C., *Phys. Rev. Lett.*, **96** (2006) 150404.
- [13] KINNUNEN J., JENSEN L.M., and TÖRMÄ P., *Phys. Rev. Lett.*, **96** (2006) 110403; YI W. and DUAN L.M., *Phys. Rev. A*, **73** (2006) 031604(R); CHEVY F., *Phys. Rev. Lett.*, **96** (2006) 130401; DE SILVA T.N. and MUELLER E.J., *Phys. Rev. A*, **73** (2006) 051602(R); HAQUE M. and STOOF H.T.C., *Phys. Rev. A*, **74** (2006) 011602(R); MARTIKAINEN J.-P., *Phys. Rev. A*, **74** (2006) 013602; CHIEN C.-C., CHEN Q., HE Y., and LEVIN K., *Phys. Rev. A*, **74** (2006) 021602(R).
- [14] YI W. and DUAN L.M., *Phys. Rev. A*, **74** (2006) 013610; PAO C.-H. and YIP S.-K., *J. Phys.: Condens. Matter*, **18** (2006) 5567.
- [15] FETTER A.L. and WALECKA J.D., *Quantum Theory of Many-Particle Systems*, (McGraw-Hill, New York) 1971.
- [16] PIERI P. and STRINATI G.C., *Phys. Rev. B*, **61** (2000) 15370.
- [17] DE GENNES P.G., *Superconductivity of Metals and Alloys*, (Benjamin, New York) 1966.
- [18] PIERI P. and STRINATI G.C., *Phys. Rev. Lett.*, **91** (2003) 030401.
- [19] SKORNIAKOV G.V. and TER-MARTIROSIAN K.A., *Sov. Phys. JETP*, **4** (1957) 648.
- [20] PETROV D.S., SALOMON C., and SHLYAPNIKOV G.V., *Phys. Rev. Lett.*, **93** (2004) 090404.
- [21] POPOV V.N., *Functional Integrals and Collective Excitations*, (Cambridge Univ. Press, Cambridge) 1987.
- [22] ZWIERLEIN M.W., ABO-SHAEER J. R., SCHIROTZKE A., SCHUNCK C.H., and KETTERLE W., *Nature*, **435** (2005) 1047.
- [23] SIMONUCCI S., PIERI P., and STRINATI G.C., unpublished.
- [24] ZWIERLEIN M.W., SCHUNCK C.H., SCHIROTZKE A., and KETTERLE W., *Nature*, **442** (2006) 54.
- [25] DE SILVA T.N. and MUELLER E. J., *Phys. Rev. A*, **73** (2006) 051602.